HHS Public Access

Author manuscript

Science. Author manuscript; available in PMC 2020 October 19.

Published in final edited form as:

Science. 2020 August 14; 369(6505): 799–806. doi:10.1126/science.abb8271.

Divergent Synthesis of Complex Diterpenes via a Hybrid Oxidative Approach

Xiao Zhang, **Emma King-Smith**, **Liao-Bin Dong**[+], **Li-Cheng Yang**, **Jeffrey D. Rudolf**[#], **Ben Shen**, **Hans Renata**[*]

Department of Chemistry, The Scripps Research Institute, 130 Scripps Way, Jupiter, FL 33458

Abstract

Polycyclic diterpenes exhibit many important biological activities, but de novo synthetic access to these molecules is highly challenging due to their structural complexity. Semisynthetic access has also been limited by the lack of chemical tools for scaffold modifications. We report a chemoenzymatic platform to access highly oxidized diterpenes by a hybrid oxidative approach that strategically combines chemical and enzymatic oxidation methods. This approach allows for selective oxidations of previously inaccessible sites on the parent carbocycles and enables abiotic skeletal rearrangements to additional underlying architectures. We synthesized a total of nine complex natural products with rich oxygenation patterns and skeletal diversity in ten steps or less from *ent*-steviol.

One Sentence Summary:

Synthesis of nine complex diterpenes through combined chemical and enzymatic C–H oxidation methods.

The *ent*-kauranes, *ent*-atisanes and *ent*-trachylobanes (Figure 1A) are biosynthetically-related families of diterpene natural products with wide-ranging biological activities (1). These activities include inhibition of ion channels, signal transduction cascades and the inflammasome (2,3,4). The main structural difference between the three natural product families lies in the carbocyclic architecture of their C/D rings: *ent*-kauranes share a common [3.2.1] bicyclic ring system while *ent*-atisanes and *ent*-trachylobanes are characterized by

[*]Correspondence to: hrenata@scripps.edu.

[+]Current address: School of Traditional Chinese Pharmacy, China Pharmaceutical University, Nanjing, 211198, China

[#]Current address: Department of Chemistry, University of Florida, Gainesville, FL 32611, USA

Author contributions: X.Z. and H.R. conceived of the work. X.Z., E.K.-S., L.-B.D., L.-C.Y., and J.D.R. designed and executed experiments. B.S. and H.R. provided insight and direction for experimental design.

Competing interests: PtmO3, PtmO5, and PtmO6 are three gene products of the platensimycin and platencin biosynthetic gene cluster, and the platensimycin and platencin biosynthetic gene cluster is included in the United States Patent No 8,652,838, titled "Platensimycin biosynthetic gene cluster of *Streptomyces platensis*", published on February 18, 2014.

Data and materials availability: All data is available in the main text or the supplementary materials.

Supplementary Materials:
Materials and Methods
Figures S1–S7
Tables S1–S19
References (40–59)
Spectral Data

the presence of a [2.2.2] bicycle and [3.2.1.0] tricycle, respectively. These three distinct ring systems are thought to arise from a common precursor (5), *ent*-copalyl pyrophosphate, through several Wagner–Meerwein shifts following initial formation of *ent*-pimarenyl cation (Figure S1). Oxidative tailoring and oxidation-enabled rearrangements could then take place on the minimally-oxidized carbocyclic skeleton, contributing to the enormous diversity found in the three natural product families. Despite recent discoveries on terpene synthases involved in the production of these families (6,7,8), most of the oxygenases that are responsible for the subsequent tailoring events have yet to be identified. Such limitations have rendered synthetic biology access to these privileged structures difficult.

Due to their intriguing architectures and promising biological activities, *ent*-kauranes, *ent*-atisanes and *ent*-trachylobanes have been the subject of many synthetic studies, more commonly through the use of *de novo* approaches (see refs. 9,10 for recent reviews; see Figure S2 for full graphical summary). Semisynthetic efforts, while not as popular, have also been pursued, including Mander's pioneering synthesis of 6,7-*seco*-*ent*-kauranes from gibberellic acid (11) and recent syntheses (12,13) of atisane-type diterpene alkaloids (e.g. **10**, Figure 1B) and neotripterifordin from stevioside. These examples suggest the possibility of developing a more systematic pursuit of highly oxidized *ent*-kauranes from stevioside, which at $0.65/g, represents an attractive starting point for synthesis. However, the realization of this concept has been hampered by the lack of useful methods for scaffold modification. As steviol (stevioside aglycone, **9**) lacks any appropriate functional handles within its A, B or C ring, semisynthetic elaborations of the framework have mostly relied on the use of C19 functionality in Hofmann–Löffler–Freytag or Suarez hypoiodite reactions (12,13), which currently only allow modification of the C20 methyl group. Remote chemical oxidation of steviol has remained unexplored, likely due to the incompatibility of its C16–C17 *exo* olefin with C–H oxidation conditions. To the best of our knowledge, such oxidation has only been performed electrochemically (14) on isosteviol ethyl ester (**11**), an *ent*-beyerane compound lacking any olefin, producing the corresponding C2-keto product. An efficient, remote, and site-selective C–H functionalization toolkit that can act on *ent*-kaurane skeleton would overcome a major roadblock in converting steviol to *ent*-kauranes containing multiple oxidations on their A, B and/or C rings (e.g. auricuoside I, Figure 1B). Furthermore, oxidized *ent*-atisanes and *ent*-trachylobanes remain hard to access using semisynthetic approaches due to the need to convert the C/D ring of *ent*-kaurane to those of *ent*-atisane and *ent*-trachylobane in a facile manner (< five steps).

We have developed a chemoenzymatic synthetic strategy to access a wide array of oxidized *ent*-kauranes, *ent*-atisanes and *ent*-trachylobanes. A key feature of this strategy is the application of a hybrid oxidative approach featuring a combination of remote biocatalytic hydroxylations and 'guided' C–H oxidation methods (15) to access to a variety of oxidation patterns previously unattainable using purely chemical means. In prior applications of C–H functionalization in natural product synthesis, each of these oxidation strategies has been employed independently (16,17), and our approach illustrates the value in combining them in a synergistic fashion. We also designed a skeletal reorganization sequence towards *ent*-atisane and *ent*-trachylobane frameworks starting from steviol (Figure 1C), which can enter analogous oxidation series to afford highly decorated members of these families. A total of

nine natural product targets were synthesized with high synthetic ideality, as well as redox- and step-economy, highlighting the enabling nature of our strategy.

Enzymatic Tool Development for Scaffold Modifications

The overarching premise of our synthetic strategy is to identify biocatalytic oxidation methods to address the methodology gap in the selective functionalization of the A, B, and C rings of minimally oxidized *ent*-kaurane, *ent*-atisane and *ent*-trachylobane skeletons. Each of the newly introduced hydroxyl groups is viewed as a gateway for further manipulations to access many members of these diterpene families through a combination of functional group interconversions and chemical C–H oxidation methods (Figure 1C). To access the *ent*-atisane and *ent*-trachylobane frameworks, we drew inspiration from the postulated biogenetic relationship between the two and the *ent*-kaurane framework. One hypothesis proposed that they arise from a common carbocation via divergent alkyl/H shifts (5). As such rearrangements could potentially be reversible in nature, we hypothesized that under suitable conditions, an *ent*-beyerane skeleton could be converted to an *ent*-atisane or *ent*-trachylobane product. Synthetic entry into this sequence could be achieved readily via the well-precedented conversion of the *ent*-kaurene stevioside to the *ent*-beyerane isosteviol (18). We postulated that further carbocation generation at C12 would trigger a Wagner–Meerwein rearrangement to an *ent*-atisane product, from which access to the *ent*-trachylobane framework could be realized via C–C bond formation between C13 and C16. Following such skeletal reorganization, an array of oxidative transformations on minimally-oxidized *ent*-atisane and *ent*-trachylobane skeleton would provide rapid access to targets such as spiramilactone C (**5**) and the mitrephorones (**7**, **8**).

Successful execution of the aforementioned strategy would thus hinge on the identification of the appropriate enzymes for selective and practical oxidations of the A, B and C rings of steviol. Prior investigations in this area (Figure S3) have not resulted in the development of synthetically-useful methods. Recent characterization of the platensimycin biosynthesis pathway has revealed the presence of several dedicated *ent*-kaurane hydroxylases for selective C–H oxidations (19,20). Early in the pathway, a P450 monooxygenase, PtmO5, catalyzes a remote C–H hydroxylation at the C11 position of *ent*-kauranol, followed by an intramolecular cyclization to form the ether bridge. Next, two functionally-redundant α-ketoglutarate-dependent dioxygenases (Fe/αKGs), PtmO3 and PtmO6, hydroxylate the C7 carbon from the β face *en route* to the construction of the enone functionality of platensimycin. If these enzymes possess sufficient substrate promiscuity to accept steviol or *ent*-kaurenoic acid as substrate, and could do so with high reaction efficiency, they would comprise ideal biocatalysts for use in our synthetic campaign. PtmO3 and PtmO6 are highly homologous (99% identical). However, the latter was better overproduced upon expression in *E. coli* and was used exclusively here. Selective C7 hydroxylation of **9** and **13** could be observed with high total turnover numbers (Figure 2), suggesting this enzyme could be useful for preparative-scale B ring oxidation of *ent*-kauranes.

Annotated as a class I P450, PtmO5 requires a separate reductase partner to support its function. We have previously employed the CamA/B reductase system for the functional characterization of PtmO5 (19) but found that this system gave very low reaction conversion

in whole-cell and lysate reactions. This observation prompted us to examine alternative reductase partners. Given prior successes (21,22), artificial fusion with a reductase partner were deemed as a particularly viable solution. Among the chimeras tested, PtmO5-RhFRed, generated by linking PtmO5 with the reductase domain of $P450_{RhF}$, provided the most promising outcome in the hydroxylation of **9** and **13**. Further co-expression of PtmO5-RhFRed, GroES/EL chaperone and the phosphite dehydrogenase Opt13 for NADPH regeneration in a single *E. coli* C41(DE3) strain allowed selective C11 hydroxylation of **9** to be attained with 88% isolated yield on preparative scale.

Variants of $P450_{BM3}$ have proven to be highly effective biocatalysts for selective oxidations of readily available terpene scaffolds (Figure S5, 23), including the A ring oxidation of decalin-containing terpenes (24,25,26,27). Furthermore, they have been shown to exhibit exceptional substrate promiscuity and excellent evolvability for new reactions. Based on these precedents, we postulated that some of these variants would be capable of performing similar oxidation on **9** or **13**. To test this hypothesis, we conducted preliminary screening of $P450_{BM3}$ alanine-scanning variants in our enzyme library (27) for the hydroxylation of **9** or **13**. No hydroxylation activity could be observed with **9**, but oxidized product(s) were formed from **13** with some of the variants tested. Variant BM3 MERO1 M177A in particular produced the C2-hydroxylated product **18** selectively without any over-oxidation or formation of C16–C17 epoxide side product. These results demonstrate the ready tunability of these oxidation biocatalysts to achieve selective reaction in the presence of other reactive functional group(s), a notable advantage over chemical oxidation methods. Importantly, this discovery identified a solution for the A ring oxidation problem.

Chemoenzymatic synthesis of oxidized *ent*-kauranes

Preliminary substrate scope examination of PtmO6, PtmO5-RhFRed and BM3 MERO1 M177A (Figure S6) suggested that they are able to accept other *ent*-kaurane and *ent*-atisane substrates bearing alternative functional group arrangements. This observation, in combination with the promiscuity of many other bacterial oxygenases (17,28) suggested that they could be useful for divergent synthesis. We initially targeted three *ent*-kauranes that would require the use of only remote B ring oxidation (Figure 3): mitrekaurenone (**21**), fujenoic acid (**23**), and pharboside aglycone (**25**). These three molecules contain different oxidation states and stereochemical configurations at C6 and C7, and their divergent synthesis would provide an ideal testbed for the synthetic versatility of biocatalytic oxidation with PtmO6. Steviol (**9**) was first converted to *ent*-kaurenoic acid (**13**) via a two-step protocol involving brominative displacement of the 3° alcohol and radical dehalogenation. The use of PtmO6 on **13** allowed selective installation of a 2° alcohol at C7, delivering the product as a single diastereomer with good conversion and yield. This transformation could be carried out routinely on gram scale using clarified lysate of *E. coli* cells expressing PtmO6. Conversion of alcohol **15** to the corresponding ketone (**20**) was accomplished by treatment with DMP. Introduction of the C6 α-OH of mitrekaurenone would require oxidation from the more hindered face of the skeleton. Thus, a strategy featuring an S_N2-type displacement of a β-disposed leaving group at C6 by the C19 acid was pursued. α-

oxidation with pyridinium tribromide was found to elicit simultaneous intramolecular lactonization by the C19 acid, thereby completing the synthesis of **21** in five steps.

To access fujenoic acid (**23**), a net ten electron oxidation needed to be carried out on the B ring of the scaffold. Chemical methods for α-hydroxy ketone synthesis were initially attempted on **20** but we fortuitously found that PtmO6 is capable of installing the C6 alcohol with superior yield. Oxidative cleavage of the C6–C7 bond with $NaIO_4$, followed by hemiketal oxidation with DMP furnished **23** in seven steps from **9**. Pharboside aglycone (**25**), on the other hand, contains a β-disposed *syn*-diol motif at C6 and C7. While **22** could potentially be a viable synthetic intermediate, the conversion of its α-hydroxy ketone functionality to the desired diol motif would require a difficult reduction from the more hindered face. As an alternative, the 2° alcohol of methyl ester **24** was dehydrated to the corresponding olefin with Burgess reagent, thereby allowing the C6,C7 *syn*-diol motif to be introduced via dihydroxylation. The use of OsO_4 and NMO simultaneously converted the two olefins to the corresponding *syn*-diol units and completed the synthesis of **25** in six steps from steviol.

Next, we sought to demonstrate the utility of our strategy in the preparation of *ent*-kauranes that contain oxidations on multiple rings (Figure 4), such as rosthornins B (**3**) and C (**30**), and fischericin B (**2**). These targets were chosen to highlight how multiple enzymatic hydroxylation reactions could be combined together or used strategically in combination with the concept of innate and guided C–H functionalization logic (15). Access to **3** and **30** from steviol would require hydroxylation at C7 and C11 with PtmO6 and PtmO5-RhFRed, reduction of the carboxylic acid at C19, and introduction of a carbonyl group at C15. To install the two alcohols at C7 and C11, a strategic decision had to be made in terms of the ordering of the two enzymatic hydroxylation steps. Performing C11 hydroxylation prior to C7 hydroxylation would necessitate nontrivial differentiation between the two alcohols for subsequent acetylation at C11 and stereochemical inversion at C7. Conversely, oxidation at C7 prior to that at C11 would allow the use of a carbonyl motif at C7 as a ‘masking’ group for the C7 α-OH and minimize potential chemoselectivity issues in subsequent manipulations. We found that ketone **26**, accessed in two steps from **9** via PtmO6 hydroxylation and PDC oxidation, could undergo a regioselective hydroxylation at C11 with PtmO5-RhFRed, albeit with only moderate conversion. Using lysates of *E. coli* expressing PtmO5-RHFRed and Opt13, C11 hydroxylation of **26** could be carried out with 65% isolated yield. The use of Ac_2O and DMAP allowed selective acetylation of the C11 alcohol without any undesired side reaction with the 3° alcohol at C13. At this stage, the C19 carboxylic acid needed to be reduced to the alcohol without concomitant removal of the acetate group at C11. This was achieved by first converting the acid to the corresponding acyl imidazole (**28**), followed by treatment with $NaBH_4$, which also led to concomitant reduction of the C7 ketone to the α-disposed alcohol. Installation of the enone unit on the D ring via selective C15–OH oxidation with SeO_2 and IBX completed the synthesis of rosthornin C (**30**) in seven steps overall. Finally, conversion of **30** to rosthornin B (**3**) could be effected via selective acetylation of the primary alcohol at C19.

Fischericin B (**2**) contains a caged ether motif that is reminiscent of platensimycin and a bridging lactone ring between C19 and C20. Synthesis of **2** would thus provide an

opportunity to develop a hybrid strategy that combines enzymatic hydroxylation at C11 and alkoxy-radical-based C–H functionalization at C20. Our synthesis commenced with PtmO5-catalyzed C11 hydroxylation of **9**. Using information gleaned from prior biosynthetic studies of platensimycin (19), the hydroxylated product could be treated with strong acidic conditions to construct the desired caged ether motif. In the presence of this motif, the C13 tertiary alcohol proved inert to conversion to the corresponding bromide for subsequent radical debromination. As a workaround, the free acid of **31** was first methylated and a Barton deoxygenation was performed on its C13 tertiary alcohol. The key hypoiodite–mediated C20 functionalization under Suarez conditions (13,29) cleanly delivered iodoaldehyde **35**, which could be further oxidized and subjected to intramolecular ring closure to complete our synthesis of fischericin B (**2**) in just nine steps.

Oxidation-enabled skeletal rearrangement to *ent*-atisane and *ent*-trachylobane

Access to minimally oxidized *ent*-atisane and *ent*-trachylobane skeletons commenced from isosteviol (**36**), an *ent*-beyerane available in one step via acid-catalyzed degradation/rearrangement of stevioside (Figure 5A). Execution of our synthetic blueprint required the installation of a functional group at C12 that is suited for subsequent carbocation generation. We envisioned first C11 hydroxylation of **36** with PtmO5-RhFRed, followed by a C11 to C12 transposition of the resulting alcohol. Hydroxylation of isosteviol with PtmO5-RhFRed unexpectedly proceeded at its C12 carbon instead of C11, thereby obviating the need for any further functional group interconversions. Furthermore, this reaction proceeded with high conversion and yield, and could be carried out routinely on multi-gram scale in a single pass. The unexpected switch in regioselectivity could be rationalized by the difference in C ring conformation of *ent*-kaurane and *ent*-beyerane. PtmO5 oxidizes the axial C11 β-H of its native substrate. In contrast, the equivalent C11 β-H on **36** adopts an equatorial configuration, and is therefore inaccessible for abstraction by the active Fe(IV)-oxo species. Instead, C–H abstraction takes place at the adjacent axial C12 β-H. Treatment of **37** with TfOH initiated the intended Wagner–Meerwein rearrangement, delivering **38**, which contains the requisite *ent*-atisane [2.2.2] C/D ring bicycle. Access to *ent*-trachylobane skeleton from **38** required the formation of a new C–C bond between C13 and C16. Examination of several different methods (30) to forge this bond led to the discovery of a reductive rearrangement in the presence of BF_3•Et_2O and Et_3SiH, which afforded an *ent*-trachylobane product **40** from **39** in 61% yield after 3x recycling. We propose that this rearrangement proceeds via ionization of C13 alcohol, followed by formation of a non-classical carbocation and selective reductive quenching at C15. Overall, this synthetic sequence provides rapid and controlled access to *ent*-atisane and *ent*-trachylobane frameworks from isosteviol in two and four steps respectively and is made possible by the use of PtmO5-catalyzed hydroxylation of **36**.

Preliminary investigation suggests that **38**, bearing high structural resemblance to the native *ent*-atiserenoic acid precursor of plantensin (6,20), is a useful intermediate for accessing more oxidized *ent*-atisanes via enzymatic hydroxylation (Figure 5B). It is capable of undergoing oxidation at C7 with PtmO6 and is hydroxylated in a more efficient fashion than

its C13-deoxy counterpart. Wolff–Kishner deoxygenation of C13 ketone and PDC oxidation of C7-OH afforded ketone **42**, which represents a potential intermediate towards spiramilactone C (**5**). In an alternative sequence, **38** could first be oxidized at C2 with BM3 MERO1 M177A to acid **43** without any observable epoxidation of its C15–C16 olefin. Wolff–Kishner reduction delivered **44**, which possesses the appropriate functionalities to be converted to the diterpenoid alkaloid cochleareine (**6**).

Chemoenzymatic synthesis of the mitrephorones

Intermediate **40** could be used to divergently prepare mitrephorones A, B and C (**7**, **49**, **8**, Figure 5C). In accord with its structural similarity to **9** or **13**, C2 oxidation of **40** with BM3 MERO1 M177A proceeded very efficiently. At high enough enzyme-to-substrate ratio, this process also led to iterative oxidation to install a ketone moiety at C2. Enzymatic oxidation with PtmO6, followed by PDC oxidation, furnished diketone **45**. As is the case with fujenoic acid (**27**), PtmO6 was capable of installing C6-OH on **45**. Intermediate **46** proved to be unstable, requiring rapid methylation of the C19 acid and mild oxidation at C6. Thus, the synthesis of mitrephorone C (**8**) was completed by methylation of the C19 acid with CH_2N_2, and further oxidation at C6 with DMP, followed by keto-enol tautomerization.

Synthesis of mitrephorone B (**49**) from **40** commenced via C7 enzymatic oxidation with PtmO6. Initial attempts focused on the dehydration of the C7-OH to the corresponding olefin, followed by a ruthenium-catalyzed direct oxidation (31) to install the C6–C7 dione moiety. Unfortunately, this sequence was found to be low yielding and accompanied by significant amounts of side-product even at low conversion. It is also worth noting that this sequence provided no desired product at all when the C2 carbon exists in the ketone oxidation state (i.e., for the mitrephorone C series). As a workaround, **40** was oxidized to the corresponding ketone (**48**), enzymatically hydroxylated at C6 with PtmO6, and then methylated and oxidized with PDC. While this route led to one more step than the dehydration/oxidation sequence, it provided a superior overall yield. According to Magauer's report (32), conversion of **49** to mitrephorone A (**7**) could be achieved through the use of electrochemical oxidation or White's Fe(PDP) catalyst. We found serendipitously that **49** is capable of undergoing a slow autoxidation to form **7** (45% yield after 7 days, or 65% yield after 14 days). Such autoxidation did not take place with **8**, suggesting that distal substituents are capable of modulating the reactivity of the diosphenol motif of **49**. This discovery allowed us to divergently prepare the entire known family members of the mitrephorones from **40**. The use of enzymatic oxidations with PtmO5-RhFRed, PtmO6 and BM3 MERO1 M177A proved to be highly enabling as all three members of the family could be prepared in less than ten steps, a marked improvement over previous routes to the mitrephorones (32,33).

Conclusion

Using this chemoenzymatic strategy, we prepared nine highly oxidized *ent*-kaurane and *ent*-trachylobane natural products in less than ten steps each. Central to this strategy is the use of three selective and scalable biocatalytic processes that are able to hydroxylate the A, B and C rings of the parent carbocyclic structures with site-selectivity and functional group

compatibility unmatched by any known small-molecule reagents or catalysts. Leveraging the newly-introduced hydroxyl groups in a series of carbocationic rearrangements enables rapid traversal of the diterpene landscape spanning the *ent*-kaurane, *ent*-atisane and *ent*-trachylobane families. By virtue of the substrate promiscuity of the enzymes, the biocatalytic oxidations can also be carefully permuted and used in conjunction with chemical C–H oxidations in multi-step synthetic sequences for streamlined access to complex natural products with minimal functional group interconversions and protecting group manipulations (34). The marriage of chemical and enzymatic C–H oxidations, in particular, constitutes a powerful means to streamline access to highly oxidized terpenes and avoids circuitous oxidative transformations, which are at times necessary in the 'two-phase' strategy for terpene synthesis (35) due to the exclusive use of small-molecule reagents or catalysts. The strategy outlined here not only opens the door for rapid access to a wide array of *ent*-kauranes, *ent*-atisanes and *ent*-trachylobanes, but also provides a blueprint for combining emerging synthetic paradigms with biocatalysis in the preparation of privileged molecular scaffolds. Generalization of this hybrid oxidative approach to other complex terpene families can be readily envisioned by way of identifying and profiling new oxygenases for site-selective modifications of building blocks (36) or late-stage functionalization (37). Finally, continued advancement in enzyme engineering strategies (38) and the development of new-to-nature transformations (39) will further expand the pool of reactions available for use and ultimately encourage broader adoption of this strategy in multi-step synthesis.

Supplementary Material

Refer to Web version on PubMed Central for supplementary material.

Acknowledgments:

We thank Profs. Phil S. Baran, Ryan A. Shenvi, Thomas J. Maimone and Keary M. Engle for useful discussions.

Funding: This work is supported, in part, by the National Institutes of Health Grant GM134954 (B.S.), GM128895 (H.R.) and GM124461 (J.D.R.).

References and Notes:

1. Liu M; Wang W-G; Sun H-D; Pu J-X Nat. Prod. Rep 2017, 34, 1090. [PubMed: 28758169]
2. Friese J; Gleitz J; Guster UT; Heubach JF; Matthiesen T; Wilffert B; Selve N Eur. J. Pharmacol 1997, 337, 165. [PubMed: 9430411]
3. Liao Y-J; Bai H-Y; Li Z-H; Zou J; Chen J-W; Zheng F; Zhang J-X; Mai S-J; Zeng M-S Sun H-D; Pu J-X; Xie D Cell Death Dis. 2014, 5, e1137. [PubMed: 24651440]
4. He H; Jiang H; Chen Y; Ye J; Wang A; Wang C; Liu Q; Liang G; Deng X; Jiang W; Zhou R Nat. Commun 2018, 9, 2550. [PubMed: 29959312]
5. Hong YJ; Tantillo DJ J. Am. Chem. Soc 2010, 132, 5375. [PubMed: 20353180]
6. Smanski MJ; Yu Z; Casper J; Lin S; Peterson RM; Chen Y; Wendt-Pienkowski E; Rajski SR; Shen B Proc. Natl. Acad. Sci. USA 2011, 108, 13498. [PubMed: 21825154]
7. Jackson AJ; Hershey DM; Chestnut T; Xu M; Peters RJ Phytochemistry 2014, 103, 13–21. [PubMed: 24810014]
8. Jin B; Cui G; Guo J; Tang J; Duan L; Lin H; Shen Y; Zhang H; Huang L Plant Physiol. 2017, 174, 943–955. [PubMed: 28381502]

9. Riehl PS; DePorre YC; Armaly AM; Groso EJ; Schindler CS Tetrahedron 2015, 71, 6629–6650.
10. Lazarski KE; Moritz BJ; Thomson RJ Angew. Chem. Int. Ed 2014, 53, 10588–10599.
11. Kenny MJ; Mander LN; Sethi SP Tetrahedron Lett. 1986, 27, 3927.
12. Cherney EC; Lopchuk JM; Green JC; Baran PS J. Am. Chem. Soc 2014, 136, 12592. [PubMed: 25159015]
13. Kobayashi S; Shibukawa K; Hamada Y; Kuruma T; Kawabata A; Masuyama A J. Org. Chem 2018, 83, 1606. [PubMed: 29328659]
14. Kawamata Y; Yan M; Liu Z; Bao D-H; Chen J; Starr JT; Baran PS J. Am. Chem. Soc 2017, 139, 7448. [PubMed: 28510449]
15. Brückl T; Baxter RD; Ishihara Y; Baran PS Acc. Chem. Res 2012, 45, 826. [PubMed: 22017496]
16. Hung K; Condakes ML; Novaes LFT; Harwood SJ; Morikawa T; Yang Z; Maimone TJ J. Am. Chem. Soc 2019, 141, 3083. [PubMed: 30698435]
17. Lowell AN; Demars MD II; Slocum ST; Yu F; Anand K; Chemler JA; Koravaki N; Priessnitz JK; Park SR; Koch AA; Schultz PJ; Sherman DH J. Am. Chem. Soc 2017, 139, 7913. [PubMed: 28525276]
18. Hutt OE; Doan TL; Georg GI Org. Lett 2013, 15, 1602–1605. [PubMed: 23530630]
19. Rudolf JD; Dong L-B; Zhang X; Renata H; Shen B J. Am. Chem. Soc 2018, 140, 12349. [PubMed: 30216060]
20. Dong L-B; Zhang X; Rudolf JD; Deng M-R; Kalkreuter E; Cepeda AJ; Renata H; Shen B J. Am. Chem. Soc 2019, 141, 4043. [PubMed: 30735041]
21. Li S; Podust LM; Sherman DH J. Am. Chem. Soc 2007, 129, 12940. [PubMed: 17915876]
22. Lu C; Shen F; Wang S; Wang Y; Liu J; Bai W-J; Wang X ACS Catal. 2018, 8, 5794.
23. Whitehouse CJC; Bell SG; Wong L-L Chem. Soc. Rev 2012, 41, 1218. [PubMed: 22008827]
24. Lewis JC; Mantovani SM; Fu Y; Snow CD; Komor RS; Wong CH; Arnold FH ChemBioChem 2010, 11, 2502–2505. [PubMed: 21108271]
25. Kille S; Zilly FE; Acevedo JP; Reetz MT Nat. Chem 2011, 3, 738–743. [PubMed: 21860465]
26. Zhang Z; El Damaty S; Fasan R J. Am. Chem. Soc 2011, 133, 3242–3245. [PubMed: 21341707]
27. Li J; Li F; King-Smith E; Renata H Nat. Chem 2020, 12, 173. [PubMed: 31959962]
28. Schmidt JJ; Khatri Y; Brody SI; Zhu C; Pietraszkiewicz H; Valeriote FA; Sherman DH ACS Chem. Biol 2020, 15, 524. [PubMed: 31961651]
29. Yu W; Hjerrild P; Overgaard J; Poulsen TB Angew. Chem. Int. Ed 2016, 55, 8294.
30. Kelly RB; Beckett BA; Eber J; Hung H-K; Zamecnik J Can. J. Chem 1975, 53, 143.
31. Kawamura S; Chu H; Felding J; Baran PS Nature 2016, 532, 90. [PubMed: 27007853]
32. Wein LA; Wurst K; Angyal P; Weisheit L; Magauer T J. Am. Chem. Soc 2019, 141, 19589–19593. [PubMed: 31770485]
33. Richter MJR; Schneider M; Brandstätter M; Krautwald S; Carreira EM J. Am. Chem. Soc 2018, 140, 16704–16710. [PubMed: 30412398]
34. Gaich T; Baran PS J. Org. Chem 2010, 75, 4657. [PubMed: 20540516]
35. Kanda Y; Nakamura H; Umemiya S; Puthukanoori RK; Appala VRM; Gaddamanugu GK; Paraselli BR; Baran PS J. Am. Chem. Soc 2020, accepted. DOI:10.1021/jacs.0c03592.
36. Hernandez-Ortega A; Vinaixa M; Zebec Z; Takano E; Scrutton NS Sci. Rep 2018, 8, 14396. [PubMed: 30258114]
37. Hong B; Luo T; Lei X ACS Cent. Sci 2020, 6, 622–635. [PubMed: 32490181]
38. Galanie S; Entwistle D; Lalonde J Nat. Prod. Rep 2020, Advance Article. DOI:10.1039/C9NP00071B.
39. Chen K; Arnold FH Nat. Catal 2020, 3, 203–213.
40. Hellwell CA; Chandler PM; Poole A; Dennis ES; Peacock WJ Proc. Natl. Acad. Sci. USA 2001, 98, 2065. [PubMed: 11172076]
41. Nett RS; Montaranes M; Marcassa A; Lu X; Nagel TC; Charles P; Hedden P; Rojas MC; Peters RJ Nat. Chem. Biol 2017, 13, 69. [PubMed: 27842068]

42. Takahashi JA; Gomes DC; Lyra FH; dos Santos GF; Martins LR Molecules 2014, 19, 1856. [PubMed: 24518806]
43. Fernando H; Halpert JR; Davydov DR Arch. Biochem. Biophys 2008, 471, 20–31. [PubMed: 18086551]
44. Munro AW Biochem. Soc. Trans 1993, 21, 216S. [PubMed: 8359466]
45. Munro AW; Lindsay JG; Coggins JR; Kelly SM; Price NC Biochim. Biophys. Acta 1996, 1296, 127–137. [PubMed: 8814218]
46. Jamakhandi AP; Jeffus BC; Dass VR; Miller GP Arch. Biochem. Biophys 2005, 439, 165–174. [PubMed: 15950923]
47. Miles JS; Munro AW; Rospendowski BN; Smith WE; McKnight J; Thomson AJ Biochem. J 1992, 288, 503–509. [PubMed: 1334408]
48. Fasan R ACS Catal. 2012, 2, 647–666.
49. Munro AW; Girvan HM; McLean KJ Biochim. Biophys. Acta 2007, 1770, 345–359. [PubMed: 17023115]
50. Sabbadin F; Hyde R; Robin A; Hilgarth E-M; Delenne M; Flitsch S; Turner N; Grogan G; Bruce NC ChemBioChem 2010, 11, 987–994. [PubMed: 20425752]
51. Sibbesen O; De Voss JJ; Ortiz de Montellano PR J. Biol. Chem 1996, 271, 22462–22469. [PubMed: 8798411]
52. Matos PM; Mahoney B; Chan Y; Day DP; Cabral MMW; Martins CHG; Santos RA; Bastos JK; Page PCB; Heleno VCG Molecules 2015, 20, 18264. [PubMed: 26457701]
53. Li C; Lee D; Graf TN; Phifer SS; Nakanishi Y; Riswan S; Setyowati FM; Saribi AM; Soejarto DD; Farnsworth NR; Falkinham JO III; Kroll DJ; Kinghorn AD; Wani MC; Oberlies NH J. Nat. Prod 2009, 72, 1949. [PubMed: 19874044]
54. Fraga BM; Gonzalez P; Hernandez MG; Suarez S Tetrahedron 2005, 61, 5623.
55. Kim KH; Choi SU; Lee KR J. Nat. Prod 2009, 72, 1121. [PubMed: 19435339]
56. Gobu FR; Chen JJ; Zeng J; Wei WJ; Wang WF; Lin CJ; Gao K J. Nat. Prod 2017, 80, 2263. [PubMed: 28783337]
57. Xu YL; Li ZQ Acta Bot. Yunnanica 1988, 20, 97.
58. Xu YL; Ma YB Phytochemistry 1989, 28, 3235.
59. Li C et al. Org. Lett 2005, 7, 5709–5712. [PubMed: 16321028]

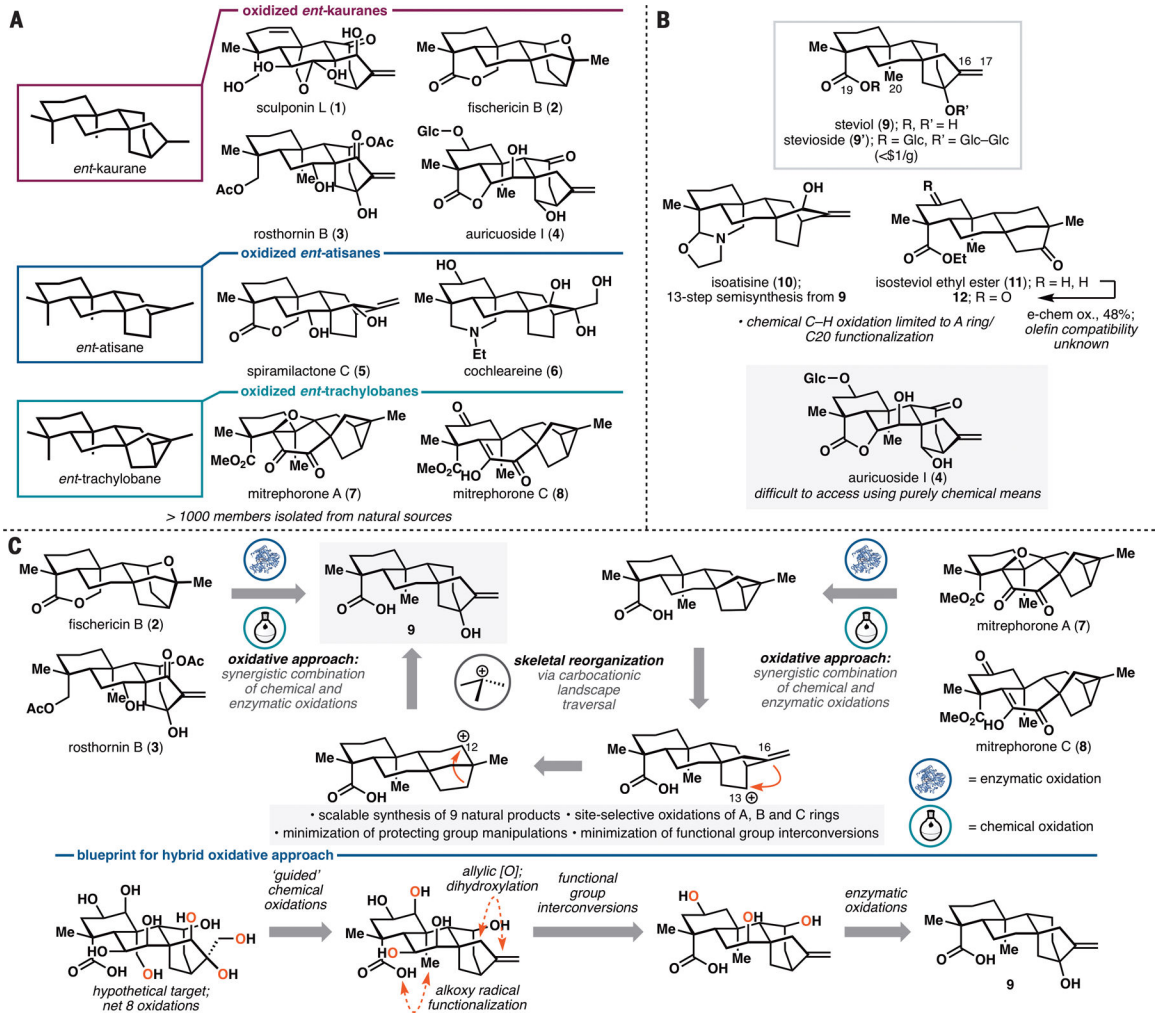

Figure 1.

A. Selected examples of oxidized *ent*-kauranes, *ent*-atisanes and *ent*-trachylobanes. **B**. Limitations of purely chemical C–H oxidation approaches in steviol-based semisynthesis. **C**. Retrosynthetic analysis of oxidized *ent*-kauranes, *ent*-atisanes and *ent*-trachylobanes employing a hybrid oxidative approach that combines chemical and enzymatic C–H oxidations. Glc = β-D-glucopyranosyl.

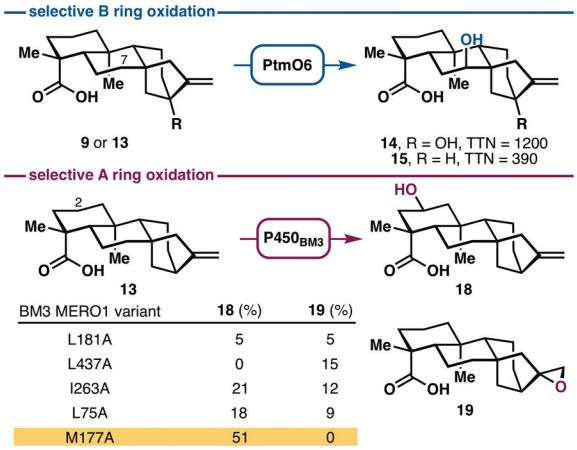

BM3 MERO1 variant	**18** (%)	**19** (%)
L181A	5	5
L437A	0	15
I263A	21	12
L75A	18	9
M177A	51	0

Substrate	Reductase Fusion	Conv. (%)
13	RhFRed	50
13	BM3Red	25
13	CamAB	<5
9	RhFRed	60
9	RhFRed	88^

Figure 2.

Discovery of three enzymes, PtmO6, PtmO5-RhFRed and BM3 MERO1 M177A for site-selective oxidations at C7, C11, and C2 respectively. See Supplementary Materials for plasmid construction (Figure S4) and reaction conditions. ^Performed by co-expressing PtmO5-RhFRed, Opt13 and GroES/EL in a single *E. coli* C41(DE3) strain.

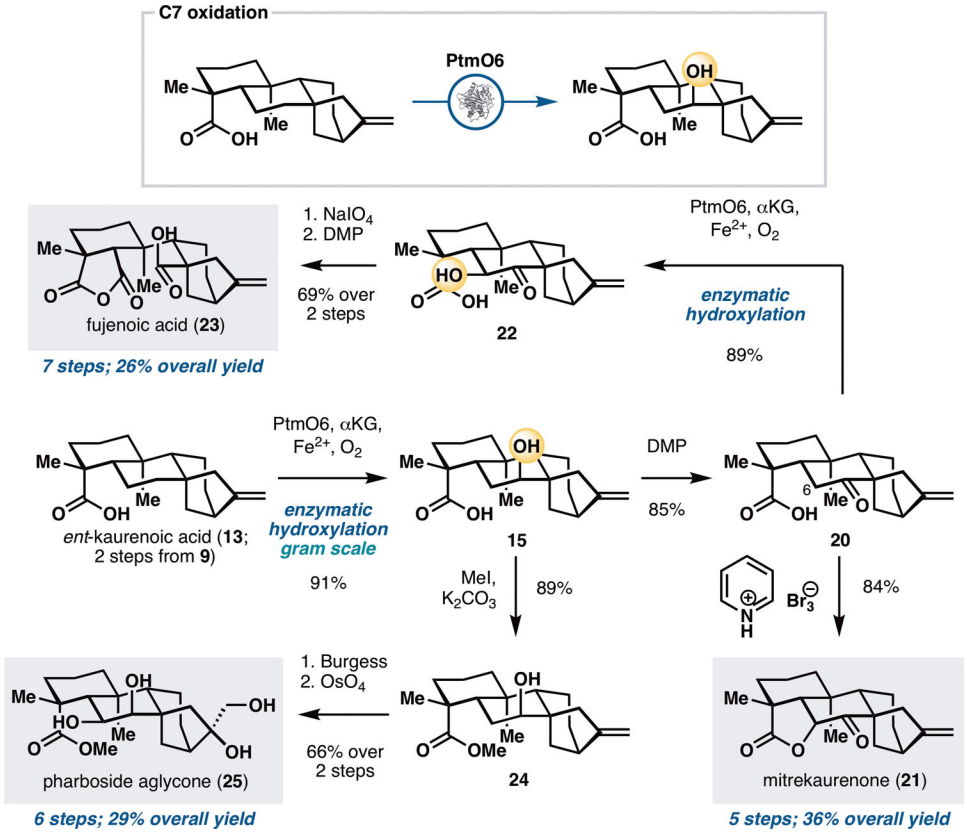

Figure 3.

Application of PtmO6 in the chemoenzymatic total synthesis of mitrekaurenone (**21**), fujenoic acid (**23**) and pharboside aglycone (**25**). See Supplementary Materials for reaction conditions.

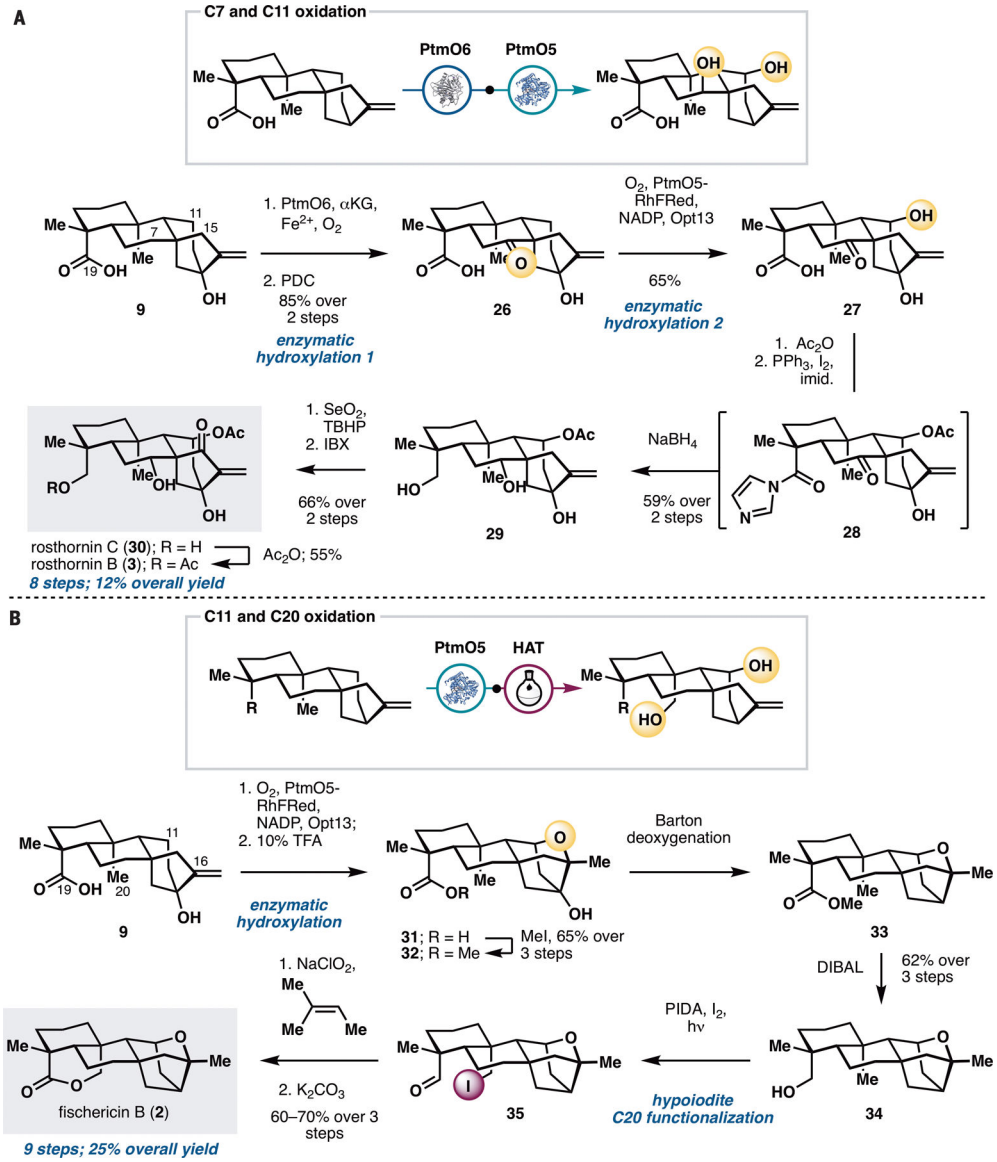

Figure 4.

Application of PtmO5-RhFRed in the chemoenzymatic total synthesis of rosthornins B (**3**) and C (**30**) and fischericin B (**2**). See Supplementary Materials for reaction conditions.

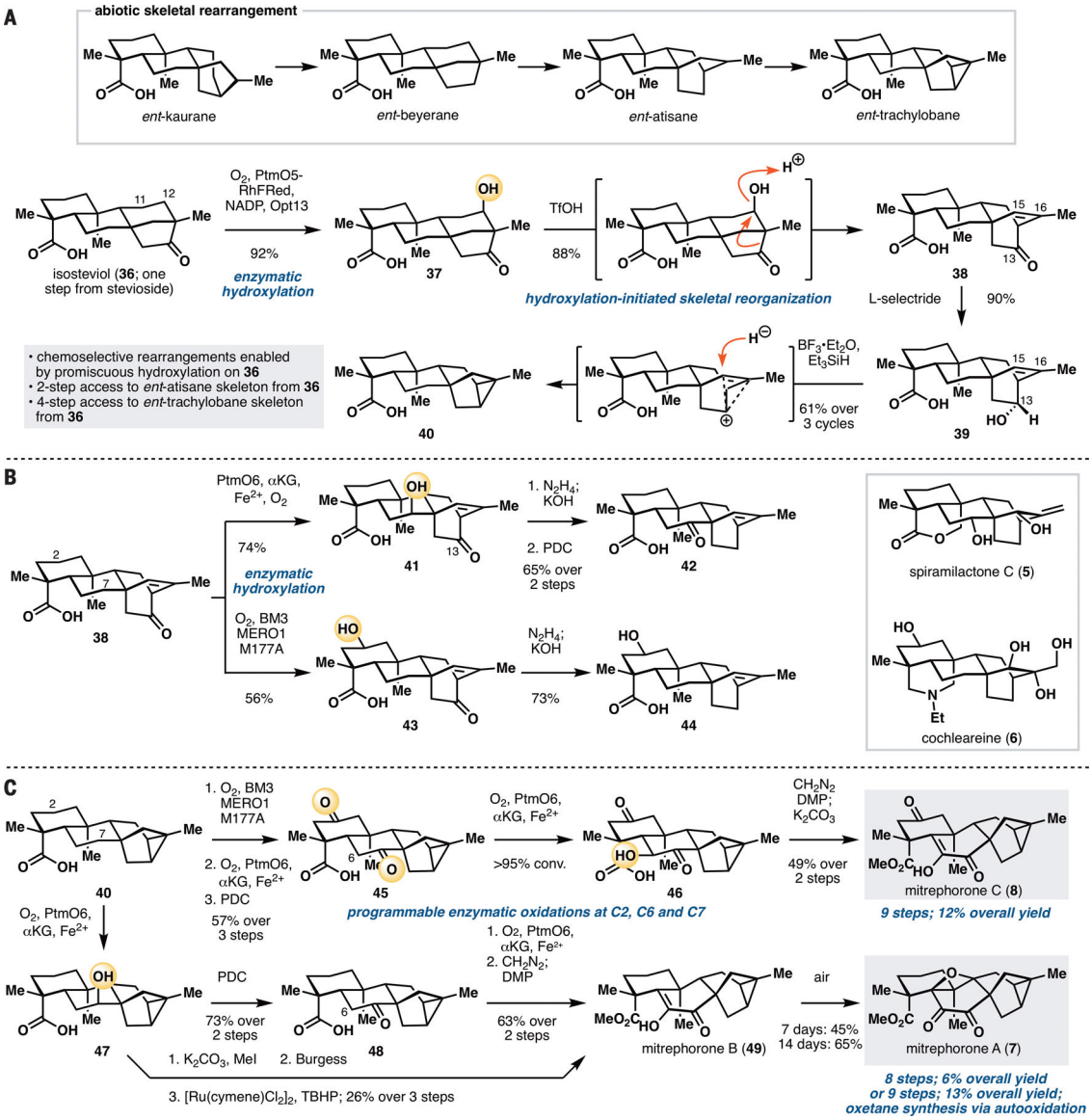

Figure 5.

A. Conversion of isosteviol (**36**) to *ent*-atisane and *ent*-trachylobane products via site-selective C12 hydroxylation and carbocationic rearrangements. **B**. Further site-selective oxidations of **38** using PtmO6 and BM3 MERO1 M177A. **C**. Divergent chemoenzymatic total synthesis of the mitrephorones starting from **40**. See Supplementary Materials for reaction conditions.